Flexibility Disaggregation under Forecast Conditions

Dominik Danner
dominik.danner@uni-passau.de
University of Passau
Passau, Bavaria, Germany

Jan Seidemann
jan.seidemann@uni-passau.de
University of Passau
Passau, Bavaria, Germany

Michael Lechl
michael.lechl@uni-passau.de
University of Passau
Passau, Bavaria, Germany

Hermann de Meer
hermann.demeer@uni-passau.de
University of Passau
Passau, Bavaria, Germany

ABSTRACT

Stationary battery energy storage systems and electric vehicles become more and more popular at households with local photovoltaic generation. Besides improving self-consumption and autarchy, these batteries can provide flexibility to an external utility. Thereby, generation and demand uncertainty, as well as cost optimality, need to be considered when utilizing distributed flexibility.

This paper discusses long short-term memory neural networks for photovoltaic generation forecast and persistence models for household load forecast with respect to their applicability in local energy management system optimization. Furthermore, a mixed-integer linear program is proposed to optimally utilize local flexible loads and storage systems. Its solution space yields the flexibility potential, which can be aggregated at flexibility pools. In order to disaggregate flexibility requests to a pool of distributed energy management systems, we propose a heuristic algorithm that can among others minimize the overall flexibility cost or maximize probability of flexibility delivery. The forecast models, the mixed integer linear program and the flexibility disaggregation are evaluated on realistic household photovoltaic and load profiles to demonstrate the full chain from local forecast to flexibility disaggregation under forecast conditions. Our experiments with flexibility disaggregation show that the probability to provide flexibility should not be neglected when it comes to distributed energy management optimization based on forecast models.

CCS CONCEPTS

• **Hardware** → **Smart grid**; • **Computing methodologies** →
Uncertainty quantification; *Neural networks*.

KEYWORDS

energy management system, forecasting, battery storage systems, electric vehicle, mixed integer linear programming, flexibility

1 INTRODUCTION

The importance of integrating renewable energy sources, such as *photovoltaic* (PV), has been rapidly increasing with the necessity of clean energy sources and long-term emission reduction [38]. However, PV generation is highly volatile, so its accurate prediction plays an essential role. Furthermore, surplus PV generation does not always match with local *Household* (HH) load demand, hence battery *Energy Storage Systems* (ESS) and flexible loads, such as plug-in *Electric Vehicles* (EVs), come into play. Managed by an *Energy Management System* (EMS), the ESS and flexible loads can be utilized for self-consumption, autarchy or cost optimization [6, 11, 19, 36], peak shaving [12], load shifting [48], or local voltage control [2, 49].

In order to optimally utilize local resources, future PV generation and household load must be known in advance. However, due to the volatile nature of weather and behavior of residents, accurate forecast becomes highly complex. Forecasting on household level introduces additional challenges, because respective profiles are even more fluctuating than for aggregated systems.

With forecast profiles of PV generation and household load, and the availability of EVs, the EMS can optimize ESS and EV profiles with respect to different objectives. On one hand, the required energy from the grid and the grid feed-in should be minimized, which contributes to a high degree of autarchy from the electric utility and to a high degree of self-consumption of own PV generation, respectively. On the other hand, EVs should be charged in blocks to avoid frequent on/off-switching operations and the ESS profile should leave the possibility to compensate forecast inaccuracies.

Besides local optimization, the EMS can offer flexibility, which is defined by ramp-up rate, power and energy [46]. We can neglect the ramp-up rate in our scenario, because we only consider ESS and EVs, whose fast converters can deliver almost instant power changes. Furthermore, *positive* flexibility refers to decreasing the grid profile, e.g. by discharging the ESS, whereas *negative* flexibility refers to increasing the grid profile, e.g. by charging the ESS. Because one single EMS cannot provide a relevant amount of flexibility, many EMSs are grouped together to form a flexibility pool. Thereby, each EMS offers its flexibility capabilities in an abstract way to avoid

privacy leaks, e.g. availability of EVs, and to be more flexible in fulfilling a flexibility request using different flexible appliances. The disaggregation strategy of such a flexibility pool should consider the total cost and probability of the flexibility to be delivered.

Many different forecast techniques are proposed in literature, among them time series [5, 18, 22, 31], linear regression [18, 22] and artificial neural networks [13, 27, 39]. However, most of them do not forecast on household level. Proposed EMS controllers only aim at local ESS optimization [6, 7] or cost-optimal EV charging [9] and, thus, do not exploit the flexibility potential on a global level. Solutions targeting flexibility provision typically do not address data privacy or uncertainty of flexibility delivery [4, 33–37, 40, 42].

In this paper we discuss a *recurrent neural network* using *long short-term memory* cells to forecast PV generation and persistence models to forecast household load in Section 3. We further define a *mixed integer linear problem* in Section 4 that optimizes the operation of an EMS with PV, ESS and EVs as flexible loads. Among others, our problem formulation considers hardware limitations arising from EV charging, e.g. controllable power limits according to IEC 61851-1, as well as utility constraints, e.g. in case discharging the ESS to the grid is prohibited. We propose a flexibility disaggregation approach in Section 5, that on one hand abstracts from the individual flexible appliances to preserve privacy and, on the other hand, considers the probability of flexibility delivery during disaggregation. The main contribution of our paper is the combination of the aforementioned three aspects: forecast models, local optimization and flexibility disaggregation. In Section 6, we perform an extensive evaluation on realistic households with PV, ESS and EVs and demonstrate the impact of forecast errors to the flexibility disaggregation to distributed EMS.

2 RELATED WORK

In this section, we provide an overview on related work in terms of forecast models and flexibility disaggregation.

2.1 Forecasting

PV generation and household load form a time series with potentially recurrent patterns. The most prevalent methods for time series forecasting are *auto-regressive* (AR), *Moving-Average* (MA) and *Autoregressive-Moving-Average* (ARMA) models [16], which are used for PV generation [5, 31, 47] and load forecast [18, 22, 25]. However, they are generally not suitable to fully capture non-stationary processes like PV generation or household load. Thus, it is required to apply differencing to the original series to obtain a stationary process, leading to *Autoregressive-Integrated-Moving-Average* (ARIMA) models. Including weather data as exogenous input improves the forecast accuracy [5]. These approaches are rather applied for aggregated profiles, where profiles of multiple PV installations (e.g. in one region) or multiple households (e.g. in one low voltage grid) are aggregated and averaged, leading to a smoother curve than for single PV installations or households [3, 30].

Recent research has been devoted to non-linear models like *Artificial Neural Networks* (ANNs), which are more flexible in capturing characteristics and relationships within data. For example a feed-forward and *Elman* neural network or *general regression* and *feed-forward backpropagation* neural network [13] is used for PV

generation forecasting. The *Long Short-Term Memory* (LSTM) cell is of special interest because it can capture sequentiality within data, which makes it suitable for PV generation forecasting [17, 27, 28]. Furthermore, a comparison of seasonal ARIMA with exogenous input and ANN-based models supports the superiority of more advanced models compared to the basic seasonal ARIMA model [47].

Similar-day models search for historical days that have similar characteristics as the forecast day. Similarity is usually determined by comparing type of days and weather conditions [10, 24, 32, 41, 45], which typically have higher impact in warmer regions [32, 45]. However, the impact of weather on the load profile in our study region is rather small and, in contrast to most existing work, we focus on forecasts of single households.

2.2 Flexibility (Dis-)Aggregation

Disaggregation algorithms aim at fulfilling a certain flexibility request by disaggregating the requested power (respectively energy) into individual profiles for prosumers. They can be differentiated according to the time horizon, for which a flexibility request is scheduled. While most disaggregate a profile comprised of multiple time slots [4, 23, 33, 37, 42, 44], few papers schedule a single time slot [34, 35, 40], which is similar to our approach.

Authors of [42] propose a disaggregation algorithm, which is based on *flex-objects* and a proportional distribution of energy. However, the disaggregation algorithm does not consider forecast uncertainties and local optimality of the underlying EMS. In contrast, flexibility is modeled as a zonotope in [33], which contains a set of feasible power trajectories that a system can follow. These enable efficient aggregation and flexibility cost functions can be used to prioritize certain trajectories, e.g. to encode local optimality. The authors of [44] model the scheduling mechanism (disaggregation) as a social welfare maximization problem over the scheduling horizon, thus contrasting the consumption benefits with the flexibility costs at the DSO level. Local optimality of the individual prosumers is considered only indirectly, but their solution deals with forecast errors by separating the scheduling mechanism into two parts: day-ahead and an intra-day scheduling.

Besides these three general approaches, some authors target more specific, demand-oriented flexibility disaggregation problems, such as EV charging [37] and residential thermal energy storage [4]. A shortcoming of their disaggregation techniques based on linear optimization is the exposure of all flexible units to the aggregator, which raises scaling and privacy concerns. Authors of [23] propose a disaggregation scheme that is based on an alternating projection method. This privacy-preserving technique, however, is not designed to provide optimal local solutions for prosumers, but just feasible ones. Our approach aims at overcoming these issues by finding a reasonable trade-off between the disclosure of prosumer information and the consideration of the prosumers' objectives.

In contrast, a disaggregation mechanism for a single time slot is proposed in [34, 35]. The required and available power flexibility in a power system is modeled with *flexibility envelopes*. The proposed linear program determines cost-optimal dispatch of generation and storage systems, such that flexibility requirements over a certain time horizon (e.g. due to renewable uncertainties) can be handled. However, global cost-optimality is not necessarily optimal for local
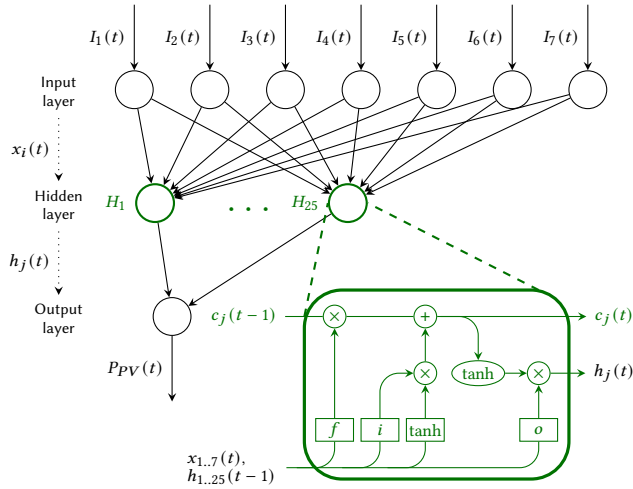
Figure 1: Structure of the three layer RNN with detailed view on a LSTM unit in the hidden layer according to [21].

ESS operators. Another flexibility model is obtained from EV characteristics [40], comprising the dimensions power, energy and time. The goal of their approach is to maximize the momentary power flexibility of a fleet of EVs with a disaggregation mechanism based on flexibility threshold paths. In our paper, we use a similar representation of power flexibility availability over time, but include the EV as flexible load within the EMS.

3 FORECAST

This section discusses forecast models for PV generation and household load, and explains the impact of uncertainty to EMS planning.

3.1 Photovoltaic Generation

A LSTM-featured *Recurrent Neural Network* (RNN) can be used to forecast the generation of a single PV installation for the next 24 hours. Our model phrases the PV generation forecast as a regression problem that predicts the PV generation at hour t using only the weather data at that time, similar to [1, 27, 29, 39]. A correlation analysis on inspected PV generation and weather data (details on the data see Section 6.1) shows the importance of 7 weather parameters with descending order of correlation: *Global Horizontal Irradiance* (GHI), *Diffuse Horizontal Irradiance* (DIF), *Direct Normal Irradiance* (DNI), *temperature*, *Direct (Beam) Horizontal Irradiance* (EBH), *Solar Zenith angle* and *Relative Humidity* (RH). These seven parameters build the input $I_1(t), \ldots, I_7(t)$ to our RNN, as shown in Figure 1. The proposed RNN is composed of three layers, one input layer with seven neurons, one hidden layer and one output layer with 1 neuron for the PV generation.

Compared to feed-forward ANNs, a RNN can store and use previously seen information from earlier time steps. However, this introduces the long-term dependency problem, where RNNs lose the ability to learn connections when the gap between the time step with relevant information and the time step where the information is needed becomes very large [20]. LSTM-RNNs overcome this problem by replacing the neurons in the hidden layer with

LSTM units, which are shown bottom right in Figure 1. Each unit H_j contains one LSTM memory cell $c_j(t)$ that stores information between time steps and three gates: The input-gate i determines to which extent a new value flows into the cell, the forget-gate f decides to which extent a value should stay in the cell, and the output-gate o determines to which extent the value in the cell contributes to the output $h_j(t)$. When at time t the input sequence $x_i(t)$ and previous output $h_j(t-1)$ is received by the three gates, activation functions within the gates determine whether the latter are triggered. Depending on the decision, $c(t)$ adapts its internal information state and the output of the LSTM unit $h_j(t)$ is finally determined by $c(t)$ and the decision of the output-gate o. With the memory cells in the different LSTM units, the interconnected cells allow the neural network to keep and forget information at the same time. Thus, LSTM-RNNs can learn both short- and long-term dependencies within data.

3.2 Household Load

Besides PV generation, we also need to forecast future household load, which can also be seen as time series. Accurate forecasting becomes challenging when dealing with single household data, since the corresponding load profiles are highly volatile, e.g. due to the behavior of the residents. Seasonal effects additionally affect the load profile, e.g. households located in the Northern Hemisphere have higher load demand during cold months, especially when they have electrical heating systems. This fact makes pattern recognition via statistical or machine learning approaches, which are typically used for aggregated load, difficult. Because our problem formulation targets single households, we consider two rather simple but effective strategies that are based on persistence modeling.

The *same-as-yesterday* (SAY) model takes the profile of the previous day as reference. The load forecast $P_{HH}(t)$ at hour t equals the recorded one $\widehat{P_{HH}}(t-24)$ and is given by Equation (1).

$$P_{HH}(t) = \widehat{P_{HH}}(t-24) \tag{1}$$

The *similar-day* (SD) model averages the load demand of similar weekdays over the last four weeks. This allows a differentiation between different weekday load patterns and the forecast load $P_{HH}(t)$ at hour t is given by Equation (2).

$$P_{HH}(t) = \text{mean}_{w=1..4}\left(\widehat{P_{HH}}(t - 24 \cdot 7 \cdot w)\right) \tag{2}$$

3.3 Uncertainty

The forecast error is calculated by subtracting the actual value from the predicted one in Equation (3) and (4) respectively. A positive error refers to a lower actual value than expected.

$$\delta_{PV}(t) = P_{PV}(t) - \widehat{P_{PV}}(t) \tag{3}$$

$$\delta_{HH}(t) = P_{HH}(t) - \widehat{P_{HH}}(t) \tag{4}$$

PV generation and household load inversely impact the total grid demand $P_G(t) = P_{HH}(t) - P_{PV}(t)$. Therefore, the combined forecast error is calculated according to Equation (5).

$$\delta(t) = \delta_{HH}(t) - \delta_{PV}(t) \tag{5}$$

For example, we assume that for an arbitrary time slot t we have an optimistic PV generation forecast of 8 kW, although the actual generation is only 5 kW. For the same time slot, we assume
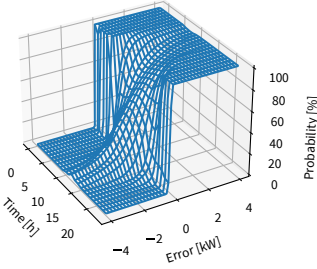
Figure 2: CDF curve of combined PV generation and load forecast error for 24 hours.

a pessimistic load forecast of 5 kW, although the actual demand is 2 kW. The positive PV forecast error $\delta_{PV}(t) = +3$ kW and the positive load forecast error $\delta_{HH}(t) = +3$ kW however result in a combined forecast error of 0 kW.

Given the error measures above and a large data set of hourly generation and load forecasts, we can calculate the error distribution function of the forecast models by applying *kernel density estimation* on the empirical distribution of the forecast error. This error distribution function defines the probability of the model to forecast with a certain error. For scheduling flexible loads in the EMS, we are mainly interested in the probability to have a certain maximum error value, which is expressed by the *Cumulative Distribution Function* (CDF). The CDF curve can be created for each individual hour of a day $P_t(X \leq x)$, as depicted in Figure 2. In the remainder of the paper, we refer to the CDF curve by the function in Equation (6) with parameters time t and error e.

$$\text{cdf}(t, e) = P_t(X \leq e) \in [0, 1] \tag{6}$$

4 EMS AND FLEXIBILITY MODELING

This section describes a detailed EMS modeling and its flexibility.

4.1 EMS Modeling

In order to maximize the use of locally generated energy from the PV system, the flexible loads need to be scheduled optimally, while considering user specific constraints such as the planned departure time of the EVs. The following MILP is defined over a discrete time horizon with T time slots of the length Δ_t and can optimize up to N EV charging processes and one battery ESS.

4.1.1   Decision Variables and Constraints. The following decision variables and parameters used in the constraints of the optimization problem are summarized in Table 1 and 2 in Appendix A.

EV charging. EV charging processes can be specified by their available time for charging ($\alpha_i(t)$), minimum required energy to be charged ($E_{EV,i}^{req}$) and hardware specific charging limitations. In European households mainly AC charging with Type-2 connectors is installed, which does not support vehicle-2-grid operation. According to IEC 61851-1, the maximum current of these charging stations is only controllable by a single variable in the range between 6 and 32 A per phase. Hence, the problem formulation must ensure that

if an EV i is charging, it charges with a minimum charging power of $P_{EV,i}^{min}$. Therefore, we define two decision variables for each time slot t and each EV charging process i.

$$M_{EV,i}(t) \in \{0, 1\} \tag{7}$$

$$P_{EV,i}(t) \in \left[0, P_{EV,i}^{max}\right] \tag{8}$$

The variable in Equation (7) encodes whether to charge ($M_{EV,i}(t) = 0$) or not ($M_{EV,i}(t) = 1$) and the variable in (8) how much power is used to charge. In order to ensure a minimum charging power the following constraint (9) must hold, which further limits $P_{EV,i}(t)$ to $\{0\} \cup [P_{EV,i}^{min}, P_{EV,i}^{max}]$.

$$P_{EV,i}^{min} \leq P_{EV,i}^{max} \cdot M_{EV,i}(t) + P_{EV,i}(t) \leq P_{EV,i}^{max} \tag{9}$$

Additionally, the constraint in Equation (10) enables EV charging only when the EV is available ($\alpha_i(t) = 1$).

$$M_{EV,i}(t) + \alpha_i(t) \geq 1 \tag{10}$$

The minimum required energy to be charged for each EV charging process is expressed with the following constraint (11), where the charging process is modeled as constant current charging with a constant efficiency factor $\mu_{EV,i}$.

$$E_{EV,i}^{req} \leq \sum_{t=0}^{T} P_{EV,i}(t) \cdot \Delta_t \cdot \mu_{EV,i} \leq E_{EV,i}^{max} - E_{EV,i}^{init} \tag{11}$$

Note that interdependence of battery state of charge between two charging processes of the same EV is not considered, because this would require a forecast of the energy consumption of the trip.

Energy Storage System. The second and most flexible appliance is the ESS. In contrast to EVs, the ESS is always available and supports bi-directional charging. In order to model charging and discharging efficiency, we define three decision variables for each time slot t.

$$M_{ESS}(t) \in \{0, 1\} \tag{12}$$

$$P_{ESS}^{+}(t) \in \left[0, P_{ESS}^{max}\right] \tag{13}$$

$$P_{ESS}^{-}(t) \in \left[0, P_{ESS}^{max}\right] \tag{14}$$

Equation (12) indicates whether to charge ($M_{ESS}(t) = 0$) or discharge ($M_{ESS}(t) = 1$) the ESS, and the variables in (13) and (14) define the charging and discharging power, respectively. To avoid charging and discharging at the same time, we add two additional constraints (15) and (16).

$$0 \leq M_{ESS}(t) \qquad \cdot P_{ESS}^{max} + P_{ESS}^{+}(t) \leq P_{ESS}^{max} \tag{15}$$

$$0 \leq (1 - M_{ESS}(t)) \cdot P_{ESS}^{max} + P_{ESS}^{-}(t) \leq P_{ESS}^{max} \tag{16}$$

Note that in this way two solutions exist for not using the ESS ($M_{ESS}(t) = 0; P_{ESS}^{+}(t) = 0$ and $M_{ESS}(t) = 1; P_{ESS}^{-}(t) = 0$), nevertheless the overall profile of the ESS which can be calculated by $P_{ESS}(t) = P_{ESS}^{+}(t) - P_{ESS}^{-}(t)$ stays the same. The time-varying stored energy in the ESS is modeled with the constraint in Equation (17), where $E_{ESS}(-1) = E_{ESS}^{init}$. The charging and discharging of the ESS uses a constant current model with efficiency factors μ_{ESS} and $\frac{1}{\mu_{ESS}}$, resulting in a round-trip storage efficiency of $(\mu_{ESS})^2$.

$$E_{ESS}(t) = E_{ESS}(t - 1)$$
$$+ \left(P_{ESS}^{+}(t) \cdot \Delta_t \cdot \mu_{ESS}\right) - \left(P_{ESS}^{-}(t) \cdot \Delta_t \cdot \frac{1}{\mu_{ESS}}\right) \tag{17}$$

Energy Management System. Finally, the EMS must operate its appliances within operational constraints. First, (time-dependent) grid limitation must be considered, e.g. limitations of the grid connection fuses or limitation of PV feed-in during certain hours. Therefore, we calculate the grid profile $P_G(t)$ using the linear equality constraint in Equation (18).

$$P_G(t) = P_{HH}(t) + \left(\sum_{i=0}^{N} P_{EV,i}(t)\right) + P_{ESS}(t) - P_{PV}(t) \quad (18)$$

The variable $P_G(t)$ is limited by constraint (19).

$$P_G^{min}(t) < P_G(t) < P_G^{max}(t) \quad (19)$$

In some countries it is not allowed to charge an ESS from the grid, or discharge to the grid in order to avoid unpredictable reverse power flows. Both can be modeled by the following two constraints (20) and (21), where $P_{diff}(t) = P_{PV}(t) - P_{HH}(t) - \sum_{i=0}^{N} P_{EV,i}(t)$.

$$P_{ESS}^+(t) \leq \quad P_{diff}(t) + M_{ESS}(t) \qquad \cdot (P_G^{max}(t) + P_{ESS}^{max}) \quad (20)$$

$$P_{ESS}^-(t) \leq -P_{diff}(t) + (1 - M_{ESS}(t)) \cdot (P_G^{min}(t) + P_{ESS}^{max}) \quad (21)$$

4.1.2 Multi-objective function. In order to optimally utilize flexibility of all local appliances, the EMS solves the MILP with the following optimization objectives with hierarchical priorities.

Cost Optimization. The main goal for the EMS is to minimize the total operational cost by minimizing the cost for buying energy from the grid, which in turn maximizes the degree of autarchy. Furthermore, utilizing local surplus PV generation optimizes self-consumption. Both are expressed by objective O_1 in Equation (22).

$$O_1 = \sum_{t=0}^{T} P_G^{buy}(t) \cdot \Delta_t \cdot c^{buy}(t)$$
$$- c^{mean} \cdot \left(E_{ESS}(T) - E_{ESS}^{init}\right) \cdot (\mu_{ESS})^2 \quad (22)$$
$$- c^{mean} \cdot \sum_{i=0}^{N} \sum_{t=0}^{T} P_{EV,i}(t) \cdot \Delta_t \cdot \mu_{EV,i}$$

We define the helper variable $P_G^{buy}(t) = \max(0, P_G(t))$, which can be encoded with linear constraints (23) and (24).

$$P_G^{buy}(t) \geq 0 \quad (23)$$
$$P_G^{buy}(t) \geq P_G(t) \quad (24)$$

In addition, the cost objective O_1 prices the stored energy in the ESS and the EVs with the average buying cost $c^{mean} = \frac{1}{T} \cdot \sum_{t=0}^{T} c^{buy}(t)$. This favors to store PV generation for later use, while load is served from the grid in case of below-average energy costs. Note that feed-in tariffs are not supported and the final objective value does not express the actual payment stream.

EV Profile Shaping. Besides cost optimization, also the shape of EV charging profiles is important, because EVs should be charged in blocks to avoid charging interrupts during the charging process. This is essential if more EVs are involved in order to avoid switching between the charging processes. Block charging can be achieved by minimizing the absolute difference between consecutive charging powers with $O_2 = \sum_{i=0}^{N} \sum_{t=0}^{T-1} |P_{EV,i}(t) - P_{EV,i}(t+1)|$. As side effect, the charging profiles will be constant as good as possible, which

is also good for the battery health. Minimization of an absolute value can be done with helper variables $B_i^+(t) \geq 0$ and $B_t^-(t) \geq 0$ and the following constraint (25).

$$P_{EV,i}(t) - P_{EV,i}(t+1) = B_i^+(t) - B_t^-(t) \quad (25)$$

The objective function O_2 is defined by (26).

$$O_2 = \sum_{i=0}^{N} \sum_{t=0}^{T-1} \left(B_i^+(t) + B_t^-(t)\right) \quad (26)$$

Peak Shaving. The EMS should have a smooth grid profile to avoid peaks at aggregation points in the power grid. Additionally, smooth grid profiles allow the EMS to compensate PV generation and household load forecast errors, because of bigger safety margins towards the grid limits. Therefore, we minimize the difference between the maximum grid consumption and the minimum grid feed-in in Equation (27). The max and min functions can be reformulated to linear equations similarly to O_1.

$$O_3 = \max_{t=0..T} (P_G(t)) - \min_{t=0..T} (P_G(t)) \quad (27)$$

EMS Flexibility. The last objective of the EMS is to utilize the ESS in a way such that it could provide maximum flexibility to compensate potential forecast errors. First, we minimize the difference between the maximum charging and discharging power of the ESS in Equation (28). Second, we keep the average SoC near to 50 % in Equation (29). In this way, we can guarantee that power and energy flexibility can be provided in both directions.

$$O_{4.1} = \left(\max_{t=0..T} \left(P_{ESS}^+(t)\right) + \max_{t=0..T} \left(P_{ESS}^-(t)\right)\right) \quad (28)$$

$$O_{4.2} = \left|\frac{1}{2}E_{ESS}^{max} - \frac{1}{T}\sum_{t=0}^{T} E_{ESS}(t)\right| \quad (29)$$

Both flexibility objectives $O_{4.1}$ and $O_{4.2}$ can be reformulated to avoid the absolute and max functions with the aforementioned techniques. Because both focus on the same decision variables, we combined them using linearization with normalization weights $\beta_1 = \frac{1}{2P_{ESS}^{max}}$ and $\beta_2 = \frac{1}{\frac{1}{2}E_{ESS}^{max}}$ to form objective O_4 in Equation (30).

$$O_4 = \beta_1 O_{4.1} + \beta_2 O_{4.2} \quad (30)$$

The overall MILP of the EMS is a multi-objective optimization problem that is solved hierarchically with decreasing prioritization in the dimensions. We first minimize O_1, add the results of O_1 as additional constraint to the problem formulation and optimize for the next objective function dimension. Thereby, the required additional amount of energy and the best time for demanding from the grid is determined first. Afterwards, the EV charging processes are scheduled in a blocked manner and the grid demand profile is shaped. Finally, the usage of the ESS is optimized to provide future flexibility. The overall MILP formulation is given by

$$\min_{x \in \text{Table 1}} (O_1, O_2, O_3, O_4)$$
$$\text{subject to} \quad (9) - (11), (15) - (21), (23), (24), (25).$$

The cost of the optimal solution can be determined by solving only the first objective O_1 due to the hierarchical optimization approach.
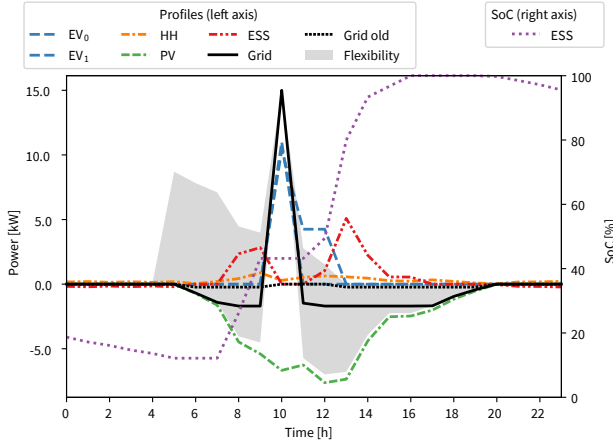
Figure 3: Power flexibility range and $-15\,\text{kW}$ flexibility scheduling at time 10. Time slot size of $1\,\text{h}$ with PV system, two EV charging process between 5-12 o'clock ($4\,\text{kW}$ to $11\,\text{kW}$ each) and an ESS with maximum of $9\,\text{kW}$.

4.2 Flexibility Modeling

The power flexibility of an EMS at time t can be defined as a variable $P_{flex}(t)$, which is limited by $P_G(t) = \widetilde{P_G}(t) - P_{flex}(t)$, where $\widetilde{P_G}(t)$ is the result of $P_G(t)$ of a previous optimization run. The upper and lower bounds of $P_{flex}(t)$ can be determined by maximizing ($P_{flex}^{max}(t) = \max_{x \in \text{Table 1}} P_{flex}(t)$) and minimizing ($P_{flex}^{min}(t) = \min_{x \in \text{Table 1}} P_{flex}(t)$) the variable accordingly. Note that in some cases a value between the boundaries of $P_{flex}(t)$ cannot be scheduled, because the only available flexible appliance is an EV, which requires a minimum power to charge. However, in most cases the ESS can compensate this small power gaps.

A power flexibility request can be assigned by fixing the flexibility variable $P_{flex}(t)$, which introduces a new constraint to the MILP. For example in Figure 3, power flexibility of $-15\,\text{kW}$ is scheduled at time 10 and possible additional flexibility is colored in gray, where negative flexibility (area above the grid profile) is mainly limited by EV availability and positive flexibility is limited by PV generation. The EMS decides on when to compensate required energy for the flexibility, which results in a grid profile with almost constant additional feed-in during PV generation in our example. If no compensation effect is desired, the flexibility request profile $P_{flex}(t)$ must be fixed to zero.

We can calculate *cost* $\gamma(x)$ and *probability* $\rho(x)$ of a flexibility request $x = P_{flex}(t)$. The cost is the difference between the cost of the optimal EMS solution before (O_1^b) and after (O_1^a) scheduling of the flexibility request. Because O_1^b is minimal, scheduling flexibility cannot yield a smaller objective result ($O_1^b \le O_1^a$) and the cost of flexibility in Equation (31) is always positive or equal to zero.

$$\gamma(x) = O_1^a - O_1^b \tag{31}$$

The probability of a flexibility request depends on the certainty of the forecast models. For example, if a positive flexibility request

is scheduled with the maximum possible flexibility of an EMS, a negative error directly impacts the probability to fulfill the flexibility request. With a margin between the scheduled flexibility and the maximum possible flexibility, additional flexibility can be used to compensate forecast errors and to deliver the planned flexibility/grid profile. Hence, the probability $\rho(x) \in [0, 1]$ of a power flexibility x can be calculated using the *cdf* function from Equation (6) and is given in Equation (32).

$$\rho(x) = \begin{cases} 1 - \text{cdf}(t, x - P_{flex}^{max}(t)) & \text{if pos flexibility} \\ \text{cdf}(t, x - P_{flex}^{min}(t)) & \text{else} \end{cases} \tag{32}$$

5 FLEXIBILITY POOLING

In order to avoid multi-indices, but still identify EMS e out of K EMS that are part of a *flexibility pool*, we define a *context* notation $[\![.]\!]_e$, where all variables inside the brackets refer to EMS e.

5.1 Flexibility Aggregation

Because the pool aggregator does not have insight into the EMS optimization, it only aggregates the power flexibility boundaries provided by the EMS, between which it assumes that flexibility requests are feasible. The power flexibility boundaries of the pool are summed up over all its EMSs in Equation (33) and (34).

$$P_{flex}^{max,Pool}(t) = \sum_{e=1}^{K} [\![P_{flex}^{max}(t)]\!]_e \tag{33}$$

$$P_{flex}^{min,Pool}(t) = \sum_{e=1}^{K} [\![P_{flex}^{min}(t)]\!]_e \tag{34}$$

Note that during disaggregation the aggregator must ensure to not assign more power flexibility to a single EMS than it can deliver.

5.2 Flexibility Disaggregation

The flexibility disaggregation of flexibility request $P_{flex}^{Pool}(t)$ to a flexibility pool is defined by a vector containing flexibility requests to each EMS of the pool $x = \left([\![P_{flex}(t)]\!]_1, \ldots, [\![P_{flex}(t)]\!]_K\right)$, where $P_{flex}^{Pool}(t) = \sum_{e=1}^{K} x_e$. A flexibility disaggregation is called feasible, if all EMS can schedule their flexibility request. Furthermore, the cost of a flexibility disaggregation x is the sum of costs of each EMS to schedule its flexibility request in Equation (35). Similarly, the probability of x is the multiplication of probabilities in Equation (36).

$$\gamma(x) = \sum_{e=1}^{K} [\![\gamma(P_{flex}(t))]\!]_e \tag{35}$$

$$\rho(x) = \prod_{e=1}^{K} [\![\rho(P_{flex}(t))]\!]_e \in [0, 1] \tag{36}$$

An optimal disaggregation should yield both, low total cost and high delivery probability. Unfortunately, this cannot be achieved using linear optimization, because the objective function might be non-linear (in case of probability of the flexibility) or can only be computed at the EMS (in case of flexibility cost). Therefore, we propose an algorithm that iteratively assigns portions of the flexibility request (with maximum size of S^{max}) to the best suitable EMS,

which is determined by a *disaggregation metric* $m(\llbracket P_{flex}(t)\rrbracket_e) \to \mathbb{R}$, until the flexibility request is fully scheduled. This disaggregation metric must decrease monotonically with increasing assigned power flexibility and different metrics are discussed in the following of this section. The disaggregation algorithm for positive flexibility is given in Algorithm 1, negative flexibility is scheduled accordingly. The algorithm starts with initializing required variables (lines 2 - 4), before iteratively assigning flexibility portions (lines 14 - 18) to the EMS with the maximum metric value, determined in lines 6 - 13. Because F is an unordered set, the EMS is randomly selected if several EMS yield the same metric value. Note that this algorithm assigns only positive requests to all EMSs and, hence, no balancing between EMSs is performed to optimize the metric value. Allowing a disaggregation vector with non-uniform signs might also imply higher total cost for the flexibility, because the additional negative flexibility must be compensated by the remaining EMSs. Furthermore, power distribution grid limitations are not considered explicitly by the disaggregation algorithm, however the feasibility of a disaggregation vector can be checked with power flow analysis, if the grid is sufficiently monitored. Alternatively, the distributed EMS should only be allowed to offer limited flexibility, e.g. by restricting the parameters $P_G^{max}(t)$ and $P_G^{min}(t)$ or by implementing concepts like flexibility lists or quotas proposed in [8].

In order to disaggregate a flexibility request $P_{flex}^{Pool}(t)$ to K EMSs, the algorithm needs to calculate the metric value once for each EMS, which we assume to be constant in $O(1)$. After assigning a flexibility portion to one EMS, only the metric value of that single EMS must be updated, other values can be cached. The number of required update steps depends on the flexibility request $P_{flex}^{Pool}(t)$ and the configured maximum step size S^{max}, and is therefore independent of K. The overall computational effort can be estimated by

$$O\left(K + \frac{P_{flex}^{Pool}(t)}{S^{max}}\right) \quad .$$

Note that the accuracy of the algorithm to achieve the expectations defined by $m(.)$ depends on S^{max} and the shape of the metric function. Smaller step sizes can improve the accuracy, but also impact the computation time.

Equal (EQUAL). With equal disaggregation, each EMS receives the absolute equal share of the flexibility request, unless it is infeasible. In that case, limited EMSs will use their maximum flexibility and the remaining EMSs have equal share of flexibility provisioning.

$$m^{EQUAL}(\llbracket P_{flex}(t)\rrbracket_e) = -\left|\llbracket P_{flex}(t)\rrbracket_e\right|$$

Proportional (PROP). With proportional disaggregation, each EMS receives a flexibility request proportional to its maximum possible flexibility. This policy ensures a proportional fair disaggregation with respect to local capabilities.

$$m^{PROP}(\llbracket P_{flex}(t)\rrbracket_e) = -\left\llbracket \frac{P_{flex}(t)}{P_{flex}^{max}(t)}\right\rrbracket_e$$

Cost-optimal (COST). With cost-optimal disaggregation, the total flexibility cost, defined in Equation (35), is heuristically minimized.

$$m^{COST}(\llbracket P_{flex}(t)\rrbracket_e) = -\llbracket \gamma(P_{flex}(t))\rrbracket_e$$

Algorithm 1: Algorithm to disaggregate positive flexibility.

> **Input:** $P_{flex}^{Pool}(t) > 0$
>
> **Data:** $m(\llbracket P_{flex}(t)\rrbracket_e) \to \mathbb{R}, S^{max} > 0$
>
> **Output:** $\left(\llbracket P_{flex}(t)\rrbracket_1, \ldots, \llbracket P_{flex}(t)\rrbracket_K\right)$

1 **if** $P_{flex}^{Pool}(t) < P_{flex}^{Pool,max}(t)$ **then**
2    $\forall e = 1..K : \llbracket P_{flex}(t) \leftarrow 0\rrbracket_e$;   // Init EMS
3    $F \leftarrow \left\{e = 1..K : \llbracket P_{flex}^{max}(t) > 0\rrbracket_e\right\}$;   // feasible EMS
4    $P_{flex}^{rem}(t) \leftarrow P_{flex}^{Pool}(t)$;   // Remaining flexibility
5   **while** $P_{flex}^{rem}(t) > 0$ **do**
6      $m_{max} \leftarrow -\infty$;
7   **foreach** $e \in F$ **do**
8        $S_e \leftarrow$
         $\min\left(S^{max}, P_{flex}^{rem}(t), \llbracket P_{flex}^{max}(t) - P_{flex}(t)\rrbracket_e\right)$;
9   **if** $m(\llbracket P_{flex}(t)\rrbracket_e + S_e) > m_{max}$ **then**
10          $m_{max} \leftarrow m(\llbracket P_{flex}(t)\rrbracket_e + S_e)$;
11          $d \leftarrow e$;   // Select EMS d
12   **end**
13   **end**
14      $\llbracket P_{flex}(t) \leftarrow P_{flex}(t)\rrbracket_d + S_d$;
15      $P_{flex}^{rem}(t) \leftarrow P_{flex}^{rem}(t) - S_d$;
16   **if** $\llbracket P_{flex}^{max}(t) = P_{flex}(t)\rrbracket_d$ **then**
17        $F \leftarrow F \setminus d$;
18   **end**
19   **end**
20 **end**

Instead of looking at the cost for scheduling each portion of flexibility ($\gamma(x + S_e) - \gamma(x)$), the total cost for scheduling the share of the EMS is considered, because the former can be non-convex and non-linear, and is not guaranteed to be monotone. On the other hand, the continuous relaxation of the MILP constraint set is convex as well as the affine linear objective function O_1. As a result, the solution space is convex (with possible gaps due to integer restrictions) and the objective function O_1 increases monotonically with increasing scheduled flexibility. The iterative algorithm will not necessarily find the optimal solution with the given metric, but it heuristically takes the EMS that provides the next flexibility portion with the lowest overall EMS cost (compared to not participating), which contributes to a low total cost.

Probability-optimal (POPT). With probability-optimal disaggregation, the overall probability from Equation (36) is maximized. Assuming that the sum of all flexibility probabilities of the EMSs is constant, all probabilities must be identical to maximize the total probability according to Lemma B.1 (see Appendix B). Hence, the first objective is to equalize the probabilities between the EMSs. Because the product of all probabilities is continuous, it is enough to reach an arbitrary near value to equality in order to obtain a value near to the maximum. Following Lemma B.2, the maximum total probability (with equal individual probabilities) is greater if the sum

of the probabilities is greater, and therefore the second objective is to maximize the sum of the probabilities. Both objectives can heuristically be achieved with the following disaggregation metric used within Algorithm 1.

$$m^{POPT}(\llbracket P_{flex}(t) \rrbracket_e) = \llbracket \rho(P_{flex}(t)) \rrbracket_e$$

Since $\rho(.)$ decreases monotonically with increasing flexibility, selecting the EMS with the highest achieved probability value will converge the probability values between EMSs as good as possible. On the other hand, if all probabilities are already close, selecting the EMS with the highest probability value will keep the sum of probabilities high.

6 EVALUATION

We first state our assumptions, present the data basis, and finally evaluate the forecast models, the MILP, and the flexibility pooling.

6.1 Assumptions and Data

Our PV generation forecast models are trained for 5 different PV systems with data from October 2017 to December 2019, excluding the four months January, April, June and October in 2019, which serve as test data. These four months are chosen to represent the different seasons of the year and were never seen by the model before. Additionally, data from February 2020 is used as validation data set to avoid overfitting of the model. We use historic weather data from *Solcast* [43] as assumed perfect weather forecast input to our models, where the most correlating weather parameters are listed in Section 3.1. The load forecast models are evaluated on load profiles of 10 different households in 2019. Both PV and load profiles are recorded by *OpenEMS* [15] at real household installations located in Central Europe and the anonymized data will be available on the *Open Energy Platform* [26].

The driving behavior of people with EVs differs to combustion engine drivers, e.g., due to smaller vehicle range, limited availability of charging facilities or because EVs are typically used as secondary car. Nevertheless, we assume that most people will not (like to) change their driving behavior drastically when switching from combustion engine vehicles to EVs in the future. Typical commuter routes will not change with the means of propulsion, and longer trips will require additional charging stops at public charging stations, which people will tend to avoid because charging at home is cheaper and much more convenient. Therefore, as basis for our EV charging profiles, we take data from the Mobility Panel Germany[1], which provides one week survey data on travel behavior in Germany [14]. We assume that hybrid PV and battery systems are more often installed in rural areas due to space limitations and that users will not charge their EVs at home if their stay is less than 1 hour. As a result, we obtain 739 daily profiles with arrival time at home, departure time and driven distance of the last trip, which must be recharged until departure. The driving distance converts to required energy $E_{EV,i}$ with the assumed energy consumption of 17 kWh per 100 km and a realistic average battery storage capacity of $E_{EV,i}^{max} = 40$ kWh. All charging processes start with an initial energy level of 10 %. The charging power of the EV is limited to values

---

[1]Mobility Panel Germany: MOP 2016/17, Bundesministerium für Verkehr und digitale Infrastruktur (English: Federal Ministry of Transport and Digital Infrastructure)
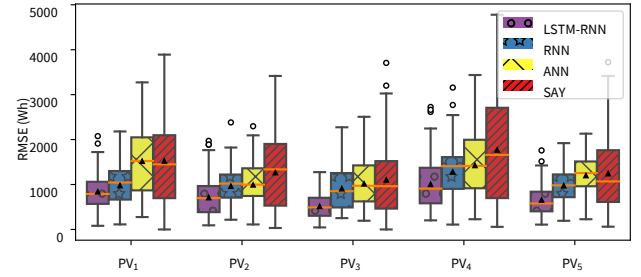
Figure 4: Daily RMSE of LSTM-RNN forecast compared to RNN, ANN and SAY approaches on the test data set.

defined by IEC 61851-1 with $P_{EV,i}^{min} = 4.3$ kW and $P_{EV,i}^{max} = 11$ kW, and a charging efficiency of $\mu_{EV,i} = 0.9$.

For each EMS, we further fix $P_G^{min}(t)$ and $P_G^{max}(t)$ to be 20 kW, assume constant energy cost, and specify a typical ESS with $P_{ESS}^{max} = 9$ kW, $E_{ESS}^{max} = 12$ kWh, $\mu_{ESS} = 0.9$ and an initial energy level of 10 %. Furthermore, we randomly assign between 0 and 2 EV charging processes to each EMS, which seems reasonable for households with up to two EVs. All simulations are carried out with quarter-hour resolution, hence $T = 96$ and $\Delta_t = 0.25$.

6.2 Forecast Models

For calculating the daily accuracy of our forecast models, we use the *Root Mean Squared Error* (RMSE) over the period of 24 h.

6.2.1 PV Generation. To compare our LSTM-RNN, we choose a RNN, a feed-forward ANN and SAY as reference models. Instead of LSTM units the RNN is configured with *SimpleRNN* units, and the ANN with *Dense* units. We apply the commonly used *Mean Squared Error* (MSE) as loss function. The LSTM units and the RNN use the default hyperbolic tangent (*tanh*) as activation function, whereas the ANN is configured with *Rectified Linear Unit* (ReLU) due to better performance with the configured loss function. The *Adam* optimizer is used as gradient descent in the backpropagation phase. The *TensorFlow Model Optimization Toolkit* optimizes the hyperparameters of our model. The best results are achieved with 30 epochs, a batch size of 17, a *L1 kernel regularizer* of 0.02, and a learning rate of 0.0189. The daily RMSE distribution of the different models is depicted in Figure 4. For all PV systems, the proposed LSTM-RNN outperforms the reference models yielding an average forecast accuracy improvement of 27.64 %, 39.52 % and 46.16 % compared to the RNN, ANN and SAY model, which seems reasonable accurate for further consideration in local optimization and flexibility disaggregation.

6.2.2 Household Load. For comparing our two persistence models, we appropriately configure the German standard load profile H0. The box plots in Figure 5 show the daily RMSE distribution and its mean value of the SD, SAY and H0 model. The SD model achieves an overall better mean RMSE for 8 out of 10 households, outperforming the SAY model by 10.3 % and the H0 standard load profile by 20 %. In contrast, the SAY model only achieves better results for 6 households compared to H0 with an overall accuracy improvement of 15.5 %. Note that the accuracy depends on the overall stability of
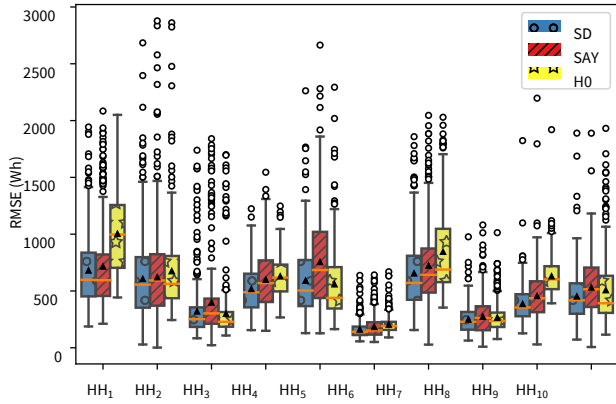
Figure 5: Daily RMSE of SD and SAY forecast compared to standard load profile in 2019.
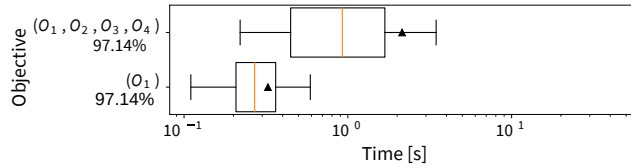

Figure 6: Computation time of 350 EMS scenarios and ratio of solvable EMS scenarios within 120s.

the load profiles. Households with rather stable load profiles (e.g. HH_6 and HH_8) have a smaller RMSE than those with more than twice the standard deviation in their daily profiles. This matches with the initial statement that load forecasting on household level is challenging especially with highly fluctuating load profiles.

PV and load forecast yield comparable error measures, however there is space for improvement, e.g. using more training data, better training setup or more sophisticated forecast models. In the following the combined forecast error is used to demonstrate the impact of local forecast errors on flexibility disaggregation, which in general is independent of the used forecast models.

6.3 EMS Model

In order to evaluate the computation time of the EMS MILP, we create 350 different realistic EMS scenarios, which are sampled from 10 household profiles, 5 PV profiles and 7 different summer days. As can be seen in Figure 6, most EMS scenario can be solved within the time limitation of 2 min on a single core of *Intel Xeon E5-2630 v4 @2.20 GHz* using *Gurobi v9.1.0*. Solving objective function O_1 for cost estimation is on average drastically faster than solving all hierarchical objective functions, which in turn positively influences the computation time of the COST flexibility disaggregation. The performance of the MILP can be quantified by the degree of self-consumption and autarchy as defined in Equation (37) and (38). The total PV generation is given by $E^{gen} = \sum_{t=0}^{T} P_{PV}(t) \cdot \Delta_t$, the feed-in power by $P_G^{sell}(t) = min(0, P_G(t))$ and the total energy consumption by $E^{con} = \sum_{t=0}^{T} \left(P_{PV}(t) + \sum_{i=0}^{N} P_{EV,i}(t) \right)$.
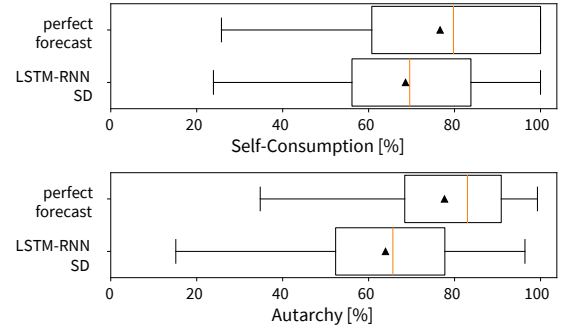
Figure 7: Self-consumption and autarchy of 350 EMS scenarios comparing forecast models with perfect forecasts.

$$self = 1 + \frac{\sum_{t=0}^{T} P_G^{sell}(t) \cdot \Delta_t}{E^{gen}} \in [0, 1] \quad (37)$$

$$aut = 1 - \frac{\sum_{t=0}^{T} P_G^{buy}(t) \cdot \Delta_t}{E^{con}} \in [0, 1] \quad (38)$$

The box plots in Figure 7 show that the MILP can not always reach maximum degree of self-consumption and autarchy even with perfect forecast, because in many EMS scenarios PV generation is smaller than the total consumption and highly misaligned with the consumption profile. Furthermore, the average degree of self-consumption is 8.04 percentage points smaller and autarchy is 13.72 percentage points smaller when using the proposed forecast models (LSTM-RNN for PV generation and SD for household load) compared to assumed perfect forecasts. However, the metric values could be improved with an online feedback controller that follows the planned ESS profile as good as possible, but limits the ESS to not charge from the grid or discharge to the grid, which occurs when naively following the optimized profiles. Consequently, forecast inaccuracies must be considered during flexibility provisioning where a scheduled power flexibility always needs to be provided.
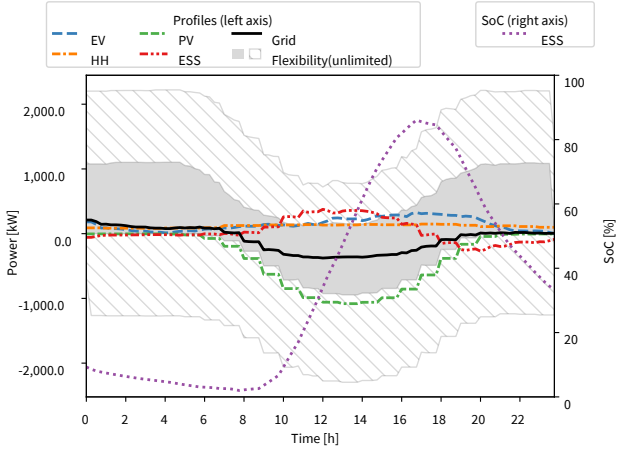
6.4 Flexibility Pooling

The EMS constraints (Equations (20) and (21)) are required to prohibit the EMS to use its ESS to participate in the energy market and cause unpredictable situations in the power distribution grid. However, these limitations drastically impact the possible flexibility that can be scheduled to an EMS. As can be seen in Figure 9, the flexibility range of a flexibility pool consisting of 150 EMSs is limited on average to only 30.37% of the maximum possible flexibility. In addition, EV charging provides mostly negative flexibility at night, and PV generation provides most positive flexibility during the day. As a result, these EMS constraints should only be used for local optimization and be neglected when it comes to flexibility scheduling in order to make maximum use of the local ESSs.

In the following, we compare the proposed disaggregation policies by analyzing a flexibility pool consisting of 150 EMS with disabled EMS constraints. Thereby, flexibility with different power levels is scheduled starting from time 10 until the flexibility pool cannot provide the required power flexibility anymore. Figure 8
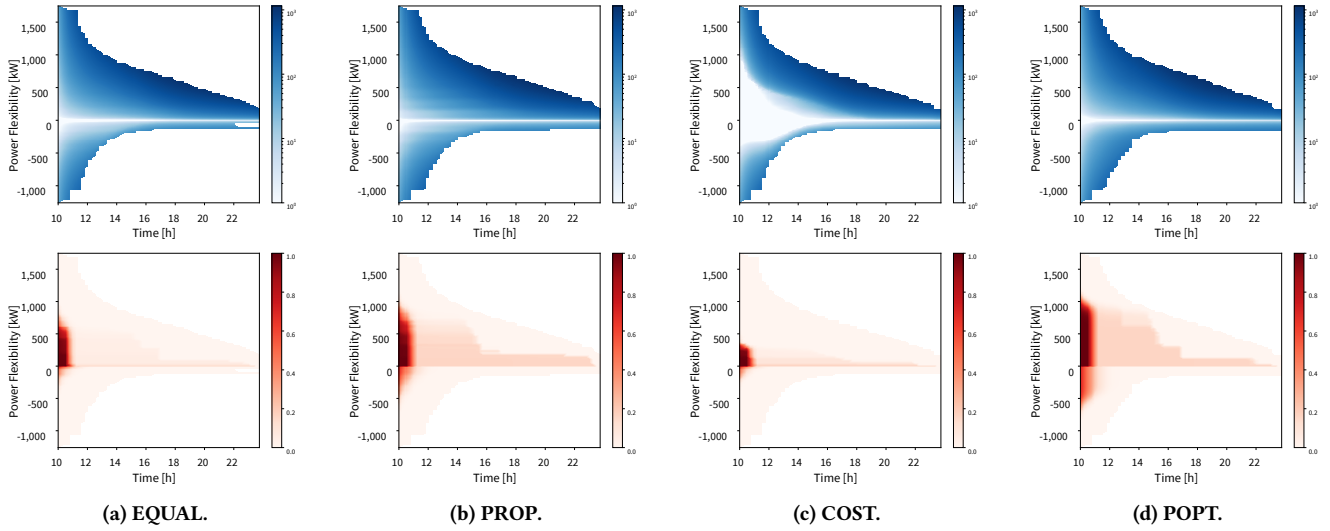
Figure 8: Aggregated cost (top, blue) and probability (bottom, red) of energy flexibility of a pool consisting of 150 EMS with $S^{max} = 1\,\mathrm{kW}$. Note that cost graphs use log scale in the color map.

Figure 9: Optimal profiles of a flexibility pool with 150 EMSs, where the background shows the different potential flexibility with (solid gray) and without (lined gray) EMS constraints.

shows cost and probability for each policy, whereby for each point in the diagram the power flexibility from the y-axis is scheduled from time 10 until the x-axis value and the color yields either total cost or delivery probability. The cost develops quite similar for all policies except for COST, which has lower total cost for small power flexibility at the beginning. Bigger differences can be seen at the probability, where POPT policy clearly outperforms EQUAL and COST. Only PROP policy achieves comparable results, because the disaggregation vector is very similar to POPT due to the similarity of the CDF curves. Consequently, cost-optimal disaggregation, as widely proposed in the literature, is not necessarily the best choice when high delivery probability is required from distributed EMSs.

7 CONCLUSION AND FUTURE WORK

In this paper we have discussed different short-term forecast models for PV generation and household load at local energy management systems, among them a LSTM-RNN for PV generation and two rather simple but easily applicable persistence models for household load. We have further defined a MILP that optimizes the local EMS operation of a stationary ESS and flexible EV charging processes. This MILP achieves a high degree of self-consumption and autarchy in day-ahead optimization, even when using forecast profiles of real household data sets. Nonetheless, the MILP is solved fast enough, such that the optimization can be deployed in a decentralized manner. The solution space of the MILP determines the possible power flexibility of the EMS, which can be aggregated at a flexibility pool. We finally proposed an iterative algorithm that performs equal, proportional, cost-optimal or probability-optimal flexibility disaggregation. Our evaluations show that limiting the usage of the ESS only for local PV over-generation, highly impacts the possible flexibility of EMSs. Finally, our simulations of flexibility disaggregation reveal that cost-optimal disaggregation is not necessarily the best choice, especially for distributed EMSs that rely on local PV and household load forecasts.

In the future, we plan to improve the forecast accuracy of the proposed models and extend the MILP formulation to support additional flexible loads, e.g. heat pumps, and ancillary services, e.g. reactive power or reserve power, which both can be modeled with additional constraints. On top of our list is an extended evaluation of the flexibility disaggregation to see how randomized flexibility requests are handled also with regard to fairness between the EMS.

ACKNOWLEDGMENTS

REFERENCES

[1] Mohamed Abuella and Badrul Chowdhury. 2015. Solar power forecasting using artificial neural networks. In *2015 North American Power Symposium (NAPS)*. IEEE, Charlotte, NC, USA, 1–5.

[2] MJE Alam, KM Muttaqi, and Darmawan Sutanto. 2012. Distributed energy storage for mitigation of voltage-rise impact caused by rooftop solar PV. In *2012 IEEE Power and Energy Society General Meeting*. IEEE, San Diego, CA, USA, 1–8.

[3] N. Amjady. 2001. Short-term hourly load forecasting using time-series modeling with peak load estimation capability. *IEEE Transactions on Power Systems* 16, 3 (2001), 498–505. https://doi.org/10.1109/59.932287

[4] M. B. Anwar, H. W. Qazi, D. J. Burke, and M. J. O'Malley. 2019. Harnessing the Flexibility of Demand-Side Resources. *IEEE Transactions on Smart Grid* 10, 4 (2019), 4151–4163. https://doi.org/10.1109/TSG.2018.2850439

[5] Peder Bacher, Henrik Madsen, and Henrik Aalborg Nielsen. 2009. Online short-term solar power forecasting. *Solar energy* 83, 10 (2009), 1772–1783.

[6] Robert Basmadjian. 2020. Optimized Charging of PV-Batteries for Households Using Real-Time Pricing Scheme: A Model and Heuristics-Based Implementation. *Electronics* 9, 1 (2020), 1–19. https://doi.org/10.3390/electronics9010113

[7] Robert Basmadjian and Hermann De Meer. 2018. A Heuristics-Based Policy to Reduce the Curtailment of Solar-Power Generation Empowered by Energy-Storage Systems. *Electronics* 7, 12 (2018), 349.

[8] BDEW. 2017. *Konkretisierung des Ampelkonzepts im Verteilungsnetz*. Technical Report. BDEW Bundesverband der Energie- und Wasserwirtschaft e.V. https://www.bdew.de/media/documents/20170210_Konkretisierung-Ampelkonzept-Smart-Grids.pdf

[9] N. Bodenschatz, M. Eider, and A. Berl. 2020. Mixed-Integer-Linear-Programming Model for the Charging Scheduling of Electric Vehicle Fleets. In *2020 10th International Conference on Advanced Computer Information Technologies (ACIT)*. IEEE, Deggendorf, Germany, 741–746. https://doi.org/10.1109/ACIT49673.2020.9208875

[10] Cai Chang-chun and Wu Min. 2008. Support vector machines with similar day's training sample application in short-term load forecasting. In *2008 Third International Conference on Electric Utility Deregulation and Restructuring and Power Technologies*. IEEE, Nanjing, China, 1221–1225. https://doi.org/10.1109/DRPT.2008.4523593

[11] Kalpesh Chaudhari, Abhisek Ukil, K Nandha Kumar, Ujjal Manandhar, and Sathish Kumar Kollimalla. 2017. Hybrid optimization for economic deployment of ESS in PV-integrated EV charging stations. *IEEE Transactions on Industrial Informatics* 14, 1 (2017), 106–116.

[12] Kein Huat Chua, Yun Seng Lim, and Stella Morris. 2016. Energy storage system for peak shaving. *International Journal of Energy Sector Management* 10, 1 (2016), 3–18. https://doi.org/10.1108/IJESM-01-2015-0003

[13] Cristian-Dragos Dumitru, Adrian Gligor, and Calin Enachescu. 2016. Solar photovoltaic energy production forecast using neural networks. *Procedia Technology* 22 (2016), 808–815.

[14] Christine Eisenmann, Ing Bastian Chlond, Tim Hilgert, Sascha von Behren, and Ing Peter Vortisch. 2017. *Deutsches Mobilitätspanel (MOP)–Wissenschaftliche Begleitung und Auswertungen Bericht 2016/2017: Alltagsmobilität und Fahrleistung*. Technical Report. KIT.

[15] Stefan Feilmeier, Wolfgang Gerbl, Fabian Schwarzbeck, Hüseyin Sahutoglu, Pooran Chandrashekaraiah, Sebastian Asen, Sagar Bandi Venu, Kyle Mclachlan, Andreas Hummelsberger, Leonid Verhovskij, Martin Grüning, Christian Lehne, Denis Jasselette, Andreas Fischer, Ante Braovic, Wolfgang Miethaner, and Jidovtseff Denis. 2021. *OpenEMS 2021.1.0*. OpenEMS. https://doi.org/10.5281/zenodo.4440884

[16] S Ferrari, M Lazzaroni, V Piuri, Loredana Cristaldi, and Marco Faifer. 2013. Statistical models approach for solar radiation prediction. In *2013 IEEE International Instrumentation and Measurement Technology Conference (I2MTC)*. IEEE, Minneapolis, MN, USA, 1734–1739. https://doi.org/10.1109/I2MTC.2013.6555712

[17] A. Gensler, J. Henze, B. Sick, and N. Raabe. 2016. Deep Learning for solar power forecasting — An approach using AutoEncoder and LSTM Neural Networks. In *2016 IEEE International Conference on Systems, Man, and Cybernetics (SMC)*. IEEE, Budapest, Hungary, 002858–002865. https://doi.org/10.1109/SMC.2016.7844673

[18] Aldo Goia, Caterina May, and Gianluca Fusai. 2010. Functional clustering and linear regression for peak load forecasting. *International Journal of Forecasting* 26, 4 (2010), 700–711. https://doi.org/10.1016/j.ijforecast.2009.05.015

[19] Hessam Golmohamadi, Reza Keypour, Birgitte Bak-Jensen, and Jayakrishnan Radhakrishna Pillai. 2019. Optimization of household energy consumption towards day-ahead retail electricity price in home energy management systems. *Sustainable Cities and Society* 47 (2019), 101468. https://doi.org/10.1016/j.scs.2019.101468

[20] S. Hochreiter. 1991. Untersuchungen zu dynamischen neuronalen Netzen. Diploma thesis, Institut für Informatik, Lehrstuhl Prof. Brauer, Technische Universität München.

[21] Sepp Hochreiter and Jürgen Schmidhuber. 1997. Long short-term memory. *Neural computation* 9, 8 (1997), 1735–1780. https://doi.org/10.1162/neco.1997.9.8.1735

[22] T. Hong, M. Gui, M. E. Baran, and H. L. Willis. 2010. Modeling and forecasting hourly electric load by multiple linear regression with interactions. In *IEEE PES General Meeting*. IEEE, Providence, RI, USA, 1–8. https://doi.org/10.1109/PES.2010.5589959

[23] P. Jacquot, O. Beaude, P. Benchimol, S. Gaubert, and N. Oudjane. 2019. A Privacy-preserving Disaggregation Algorithm for Non-intrusive Management of Flexible Energy. In *2019 IEEE 58th Conference on Decision and Control (CDC)*. IEEE, Nice, France, France, 890–896. https://doi.org/10.1109/CDC40024.2019.9029991

[24] Amit Jain and B Satish. 2009. Clustering based short term load forecasting using support vector machines. In *2009 IEEE Bucharest PowerTech*. IEEE, Bucharest, Romania, 1–8. https://doi.org/10.1109/PTC.2009.5282144

[25] Kyung-Bin Song, Young-Sik Baek, Dug Hun Hong, and G. Jang. 2005. Short-term load forecasting for the holidays using fuzzy linear regression method. *IEEE Transactions on Power Systems* 20, 1 (2005), 96–101. https://doi.org/10.1109/TPWRS.2004.835632

[26] Michael Lechl and Stefan Feilmeier. 2021. *EMSIG: Energy Management System Data*. OpenEMS Association e.V. https://openems.io/research/emsig/

[27] Donghun Lee and Kwanho Kim. 2019. Recurrent neural network-based hourly prediction of photovoltaic power output using meteorological information. *Energies* 12, 2 (2019), 215.

[28] Gangqiang Li, Huaizhi Wang, Shengli Zhang, Jiantao Xin, and Huichuan Liu. 2019. Recurrent neural networks based photovoltaic power forecasting approach. *Energies* 12, 13 (2019), 2538.

[29] Elke Lorenz, Johannes Hurka, Detlev Heinemann, and Hans Georg Beyer. 2009. Irradiance forecasting for the power prediction of grid-connected photovoltaic systems. *IEEE Journal of selected topics in applied earth observations and remote sensing* 2, 1 (2009), 2–10.

[30] H. Matsila and P. Bokoro. 2018. Load Forecasting Using Statistical Time Series Model in a Medium Voltage Distribution Network. In *IECON 2018 - 44th Annual Conference of the IEEE Industrial Electronics Society*. IEEE, Washington, DC, USA, 4974–4979. https://doi.org/10.1109/IECON.2018.8592891

[31] A. El Mouatasim and Y. Darmane. 2018. Regression analysis of a photovoltaic (PV) system in FPO. In *AIP Conference Proceedings*, Vol. 2056. AIP Publishing LLC, AIP Publishing LLC, Ouarzazate, Morocco, 020008. https://doi.org/10.1063/1.5084981

[32] Qingqing Mu, Yonggang Wu, Xiaoqiang Pan, Liangyi Huang, and Xian Li. 2010. Short-term load forecasting using improved similar days method. In *2010 Asia-Pacific Power and Energy Engineering Conference*. IEEE, Chengdu, China, 1–4. https://doi.org/10.1109/APPEEC.2010.5448655

[33] Fabian L Müller, Jácint Szabó, Olle Sundström, and John Lygeros. 2017. Aggregation and disaggregation of energetic flexibility from distributed energy resources. *IEEE Transactions on Smart Grid* 10, 2 (2017), 1205–1214.

[34] Hussam Nosair and Franois Bouffard. 2015. Flexibility envelopes for power system operational planning. *IEEE Transactions on Sustainable Energy* 6, 3 (2015), 800–809.

[35] Hussam Nosair and François Bouffard. 2016. Energy-centric flexibility management in power systems. *IEEE Transactions on Power Systems* 31, 6 (2016), 5071–5081.

[36] S. Ostovar, M. Moeini-Aghtaie, and M. B. Hadi. 2020. Developing a New Flexibility-Based Algorithm for Home Energy Management System (HEMS). In *2020 10th Smart Grid Conference (SGC)*. IEEE, Kashan, Iran, 1–6. https://doi.org/10.1109/SGC52076.2020.9335730

[37] Michael Pertl, Francesco Carducci, Michaelangelo Tabone, Mattia Marinelli, Sila Kiliccote, and Emre C Kara. 2018. An equivalent time-variant storage model to harness ev flexibility: Forecast and aggregation. *IEEE Transactions on Industrial Informatics* 15, 4 (2018), 1899–1910.

[38] REN21. 2016. *Renewables 2016 Global status report*. Technical Report. REN21. https://www.ren21.net/gsr-2016/

[39] Aminmohammad Saberian, H Hizam, MAM Radzi, MZA Ab Kadir, and Maryam Mirzaei. 2014. Modelling and prediction of photovoltaic power output using artificial neural networks. *International Journal of Photoenergy* 2014 (2014), 1–10. https://doi.org/10.1155/2014/469701

[40] Jonas Schlund, Marco Pruckner, and Reinhard German. 2020. FlexAbility - Modeling and Maximizing the Bidirectional Flexibility Availability of Unidirectional Charging of Large Pools of Electric Vehicles. In *Proceedings of the Eleventh ACM International Conference on Future Energy Systems (e-Energy '20)*. Association for Computing Machinery, Virtual Event, Australia, 121–132. https://doi.org/10.1145/3396851.3397697

[41] Tomonobu Senjyu, Hitoshi Takara, Katsumi Uezato, and Toshihisa Funabashi. 2002. One-hour-ahead load forecasting using neural network. *IEEE Transactions on power systems* 17, 1 (2002), 113–118. https://doi.org/10.1109/PTC.2009.5282144

[42] Laurynas Šikšnys, Emmanouil Valsomatzis, Katja Hose, and Torben Bach Pedersen. 2015. Aggregating and disaggregating flexibility objects. *IEEE Transactions on Knowledge and Data Engineering* 27, 11 (2015), 2893–2906.

[43] Solcast. 2020. *Solar Irradiance Data*. Solcast. https://solcast.com

[44] Shahab Shariat Torbaghan, Niels Blaauwbroek, Dirk Kuiken, Madeleine Gibescu, Maryam Hajighasemi, Phuong Nguyen, Gerard JM Smit, Martha Roggenkamp, and Johann Hurink. 2018. A market-based framework for demand side flexibility scheduling and dispatching. *Sustainable Energy, Grids and Networks* 14 (2018), 47–61.

[45] Carolina Tranchita and Alvaro Torres. 2004. Soft computing techniques for short term load forecasting. In *IEEE PES Power Systems Conference and Exposition, 2004.* IEEE, New York, NY, USA, 497–502. https://doi.org/10.1109/PSCE.2004.1397459

[46] A. Ulbig and G. Andersson. 2012. On operational flexibility in power systems. In *2012 IEEE Power and Energy Society General Meeting*. IEEE, San Diego, CA, USA, 1–8. https://doi.org/10.1109/PESGM.2012.6344676

[47] Stylianos I Vagropoulos, GI Chouliaras, Evaggelos G Kardakos, Christos K Simoglou, and Anastasios G Bakirtzis. 2016. Comparison of SARIMAX, SARIMA, modified SARIMA and ANN-based models for short-term PV generation forecasting. In *2016 IEEE International Energy Conference (ENERGYCON)*. IEEE, Leuven, Belgium, 1–6. https://doi.org/10.1109/ENERGYCON.2016.7514029

[48] Sergio Vazquez, Srdjan M Lukic, Eduardo Galvan, Leopoldo G Franquelo, and Juan M Carrasco. 2010. Energy storage systems for transport and grid applications. *IEEE Transactions on industrial electronics* 57, 12 (2010), 3881–3895.

[49] Jan Von Appen, Thomas Stetz, Martin Braun, and Armin Schmiegel. 2014. Local voltage control strategies for PV storage systems in distribution grids. *IEEE Transactions on Smart Grid* 5, 2 (2014), 1002–1009.

A APPENDIX

Table 1: MILP decision variables grouped by appliance.

Variable		Description
$M_{EV,i}(t)$	$\in \{0,1\}$	Charge (0) or not (1)
$P_{EV,i}(t)$	$\in \left[0, P_{EV,i}^{max}\right]$	Charging power of EV i
$M_{ESS}(t)$	$\in \{0,1\}$	Charge (0) or discharge (1)
$P_{ESS}^{+}(t)$	$\in \left[0, P_{ESS}^{max}\right]$	Charging power of the ESS
$P_{ESS}^{-}(t)$	$\in \left[0, P_{ESS}^{max}\right]$	Discharging power of the ESS
$E_{ESS}(t)$	$\in \left[0, E_{ESS}^{max}\right]$	Stored energy in the ESS

Table 2: MILP parameters grouped by appliance.

Parameter		Description
t	$= 0..T$	Index for time slot t out of T time slots
i	$= 0..N$	Index for EV charging process i out of N
Δ_t	> 0	Size of the time slot [h]
$c^{buy}(t)$	> 0	Time-dependent energy cost [ct/kWh]
$P_{PV}(t)$	≥ 0	Time-dependent PV production [kW]
$P_{HH}(t)$	≥ 0	Time-dependent HH load [kW]
$P_G^{max}(t)$	≥ 0	Time-dependent upper grid limit [kW]
$P_G^{min}(t)$	≤ 0	Time-dependent lower grid limit [kW]
$\alpha_i(t)$	$\in \{0,1\}$	EV is available (1) or not (0)
$\mu_{EV,i}$	$\in (0,1]$	Efficiency of EV charging
$P_{EV,i}^{min}$	≥ 0	Minimum EV charging power [kW]
$P_{EV,i}^{max}$	$\geq P_{EV,i}^{min}$	Maximum EV charging power [kW]
$E_{EV,i}^{req}$	> 0	EV energy requirement [kWh]
$E_{EV,i}^{init}$	≥ 0	Initially stored energy of EV [kWh]
$E_{EV,i}^{max}$	$> E_{EV,i}^{init}$	Maximum energy storage of EV [kWh]
μ_{ESS}	$\in (0,1]$	Efficiency of the ESS
P_{ESS}^{max}	≥ 0	Maximum power of the ESS [kW]
E_{ESS}^{init}	≥ 0	Initially stored energy of the ESS [kWh]
E_{ESS}^{max}	≥ 0	Maximum energy storage of the ESS [kWh]

B APPENDIX

LEMMA B.1. *Let $K \in \mathbb{R}_0^+$, $a_1, \ldots, a_n \in \mathbb{R}_0^+$ such that $\sum_{i=1}^{n} a_i = K$ and $f \colon \mathbb{R}^n \to \mathbb{R} \colon (a_1, \ldots, a_n) \mapsto \prod_{i=1}^{n} a_i$*

$$\forall i = 1..n : a_i = \frac{K}{n} \text{ assumes a maximum in } f(a_1, \ldots, a_n)$$

PROOF. Assume there is a vector $(b_1, \ldots, b_n)$ that yields maximum value for $\prod_{i=1}^{n} b_i$, but has different values at indices k and m, $k \neq m$. Let $d > 0$, $b_k = \frac{K}{n} - d$ and $b_m = \frac{K}{n} + d$, than $b_k \cdot b_m = \left(\frac{K}{n}\right)^2 - d^2 < \left(\frac{K}{n}\right)^2$, hence $\prod_{i=1}^{n} b_i$ not maximal. □

LEMMA B.2. *Let $K_1, K_2 \in \mathbb{R}_0^+$, $K_1 < K_2$, $a_1, \ldots, a_n, b_1, \ldots, b_n \in \mathbb{R}_0^+$ such that $\sum_{i=1}^{n} a_i = K_1$ and $\sum_{i=1}^{n} b_i = K_2$*

$$\max_{a_1, \ldots, a_n} \prod_{i=1}^{n} a_i < \max_{b_1, \ldots, b_n} \prod_{i=1}^{n} b_i$$

PROOF. Let $a_1, \ldots, a_n$ be values that yield the maximum for $\prod_{i=1}^{n} a_i$ and $\sum_{i=1}^{n} a_i = K_1$. Define $\forall i = 1..(n-1) : b_i = a_i, b_n = a_n+1$ and $\sum_{i=1}^{n} b_i = K_2$, than obviously $K_1 < K_2$ and

$$\max_{a_1, \ldots, a_n} \prod_{i=1}^{n} a_i = a_n \prod_{i=1}^{n-1} a_i < (a_n + 1) \prod_{i=1}^{n-1} a_i = \prod_{i=1}^{n} b_i \leq \max_{b_1, \ldots, b_n} \prod_{i=1}^{n} b_i$$

□